Nano Research 2015, 8(7): 2351–2362
DOI 10.1007/s12274-015-0745-7
Research Article
ISSN 1998-0124
CN 11-5974/O4

Mesoporous Ag nanocubes synthesized via selectively oxidative etching at room temperature for surface-enhanced Raman spectroscopy

Lin Gan[1], Meijia Yang[1], Xi Ke[2], Guofeng Cui[2] (✉), Xudong Chen[1] (✉), Shiva Gupta[3], William Kellogg[3], Drew Higgins[4], and Gang Wu[3]

[1] *Key Laboratory for Polymeric Composite and Functional Materials of Ministry of Education of China, Sun Yat-sen University, Guangzhou 510275, China*
[2] *Electronic Packaging Electrochemistry Laboratory, School of Chemistry and Chemical Engineering, Sun Yat-sen University, Guangzhou 510275, China*
[3] *Department of Chemical and Biological Engineering, University at Buffalo, The State University of New York, Buffalo, New York 14260, USA*
[4] *Department of Chemical Engineering, University of Waterloo, Waterloo, Ontario, N2L 3G1, Canada*

Received: 20 December 2014
Revised: 1 February 2015
Accepted: 10 February 2015

KEYWORDS
Ag nanocube,
selective etching,
water phase synthesis,
room temperature,
surface-enhanced Raman scattering (SERS)

ABSTRACT

Silver nanocubes enriched with {100} facets have been extensively used for surface-enhanced Raman scattering. Herein, we report a new water-phase synthesis method for well-defined Ag nanocubes with tunable sizes via a two-step procedure at room temperature. First, irregularly shaped Ag nanoparticles (INPs) were prepared by reducing silver ammonia solution using ethylal. Second, the agglomerated INPs were selectively etched with HNO_3 and Cl^- to yield {100} facet-rich mesoporous Ag nanocubes. The mechanism of Ag-nanocube formation and growth was investigated in detail by elucidating the involved chemical reactions and physical changes at each step during the synthesis. The addition of Cl^- anions was responsible for facilitating Ag nanoparticle growth by removing surface-adsorbed Ag^+ species, thereby eliminating inter-particle repulsive forces. This agglomeration was found crucial for the subsequent selective oxidation of Ag nanoparticles because the protective agent used, polyvinylpyrrolidone (PVP), was the most effective one for adsorption on the surfaces of Ag nanoparticles of size greater than approximately 50 nm. Importantly, mesopores were found inside the Ag nanocubes; this can be attributed to the unavoidable imperfect packing during the agglomeration of INPs. The newly prepared Ag nanocubes were further used to enhance the Raman signal of rhodamine 6G, which is capable of reducing the detection limitation to 10^{-16} mol·L^{-1}.

Address correspondence to Guofeng Cui, cuigf@mail.sysu.edu.cn; Xudong Chen, cescxd@mail.sysu.edu.cn

1 Introduction

Silver nanocubes have received widespread interest owing to their unique {100} facets and intriguing surface plasmonic properties [1–4]. It is known that when silver nanocrystals are used in optical or photovoltaic devices, the nanoparticle spacing is an important parameter that influences their localized surface plasmonic resonance (LSPR) properties [5–7]. The smooth and regular surfaces of nanocubes enable their easy self-assembly into ordered 2D arrays [8], with the nanoparticle spacing of the silver nanocubes in the 2D arrays controllable through deposition at different surface pressures via the Langmuir–Blodgett method [9–13]. Additionally, this inter-particle coupling can be tuned over a large area, rendering silver nanocubes highly reactive and practical substrates for application in various fields including surface-enhanced Raman scattering (SERS) [10–12, 14], sensors [15, 16], and fluorescence devices [17, 18]. Furthermore, silver nanocubes have a large number of surface atoms on the edge of {100} facets, which can provide intriguing catalytic features [19, 20]. Thus, the application of silver nanocubes has recently been extended to the field of catalysis because of their high electrocatalytic activity in comparison to truncated cubes and spheres [21, 22]. Silver atoms on the {100} facets show unique chemical activity, which has been used to synthesize cubic Au nanocages with pores at all corners [23], along with nanoframes without wall structures [24]. A unique Ag@Ni core-shell structure has been synthesized using silver nanocubes as the growth substrates owing to their unique lattice parameters of the Ag {100} facets that facilitate an unusual epitaxial growth of Ni particles on their surface [25].

Among the many explored synthesis methods, most, however, involve the formation of Ag nanocubes at high temperatures (usually higher than 140 °C) employing polyols (e.g., ethylene glycol) as the solvent [26–30]. Furthermore, these toxic polyols have to be heated for long periods (e.g., 1 h) to generate aldehyde reductants. Additionally, the reaction kinetics during Ag nanocube growth is so rapid that the careful tuning of the overall process and termination of the reaction are problematic to control. Hence, it is difficult to achieve Ag nanoparticles with consistent size distributions, morphology, and properties. These methods also consume large amounts of energy and require large amounts of expensive organic solvents. Thus far, the reported synthesis methods of Ag nanocubes using a water phase rely on high temperatures (e.g., 120 °C) and high pressures [31, 32]. If the synthesis temperature decreases to room temperature, the prepared nanoparticles are usually spherical [33–35], and the synthesis procedures are not transferrable to the preparation of nanocubes. Hence, it is still a great challenge to develop a water-phase method for the synthesis of Ag nanocubes at room temperature with controlled sizes.

Herein, we developed a facile and low-cost water-phase approach to synthesize Ag nanocubes through the selective oxidative etching of irregularly shaped silver nanoparticles (INPs) at room temperature. Ag INPs were first prepared by rapidly reducing silver ammonia solution using ethylal. Then, the as-prepared INPs were etched using diluted HNO_3 solution. During the etching process, polyvinylpyrrolidone (PVP) was strongly adsorbed on the Ag {100} facets, thereby protecting them and allowing for selectively etching the Ag INPs. As a result, the Ag nanoparticles evolved to nanocubes enclosed by well-defined Ag {100} facets. During this process, the INPs were not only etched but also agglomerated during the shape evolution process because of their high surface energy [36]. It was found that Cl^- could be added to remove surface Ag^+ species, providing control on the agglomeration and improvements to the size and shape monodispersity. Moreover, Cl^-/oxygen (from air) acted as an oxidative etching reagent for increasing the etching and shape evolving rate. Additionally, mesopores were detected inside the Ag nanocubes by the N_2 adsorption isotherm, and we attribute them to the unavoidable imperfect packing during the agglomeration of Ag INPs.

The prepared Ag nanocubes were applied in the SERS field. The SERS enhancement factor for the Raman signal of rhodamine 6G (R6G) can be up to 10^{13} with the substrate consisting of Ag nanocubes, and the detection limit can be as low as 10^{-16} mol·L^{-1}; the detection limit of R6G with Ag nanocubes synthesized via conventional high temperature/glycol method was measured to be 10^{-12} mol·L^{-1}.

2 Experimental section

2.1 Two-step synthesis of Ag nanocubes

In the preparation of Ag nanocubes, the first step involved the preparation of Ag INPs. We added 50 mL of a 150 mmol·L^{-1} aqueous PVP solution into a 150 mL round bottom flask under strong magnetic stirring at room temperature, and then 1.0 mL of $AgNO_3$ (700 mmol·L^{-1} in water) and 400 μL of ethylal (35 wt.% in water) solutions were injected. After 20 min, 10 μL of 25 wt.% aqueous ammonia was injected into the solution, turning the color of the dispersion to red after ~2 min and making the UV absorption peak of the dispersion appear at approximately 420 nm. In the second step, HNO_3 was used to adjust pH value of the solution to ~1.5. After stirring for 20 min, 20 μL of 1 mol·L^{-1} NaCl aqueous solution was injected, and the resulting solution was held for 40 min. Finally, Ag nanocubes were obtained after subsequent centrifugation; washing twice each with acetone, ethylol, and deionized (DI) water; and storing in 25 mL DI water.

2.2 Growth mechanism investigation

To study the growth mechanism of the Ag nanocubes, we separated the aforementioned two-step procedure. First, we prepared the Ag INPs using the method described previously. However, when the dispersion turned red or reddish black and the UV absorption peak appeared at approximately 420 nm after the addition of ammonia, the reaction was quenched with 10 μL acetic acid. The products were then separated by centrifugation and washed twice each with acetone, ethylol, and DI water. The resulting INPs were then stored in 25 mL DI water. In the second step, 25 mL of PVP (300 mmol·L^{-1} in water) was added into a 150-mL round bottom flask under vigorous magnetic stirring at room temperature, and 25 mL of the as-prepared Ag INP dispersions was injected. Thus, there was no reductant in the reacting solution. Subsequently, the pH was modified to ~1.5 with HNO_3, and held for either (i) ~4 h or (ii) 20 min, followed by the addition of 20 μL of 1 mol·L^{-1} NaCl aqueous solution; the mixture was then held for 40 min. The remaining steps are identical to those of the regular synthesis procedures.

2.3 Characterization

Scanning electron microscope (SEM) images were obtained with a Hitachi S4800 at a beam energy of 10.0 kV. The size distributions were deduced from the statistical analysis of 200 particles from SEM images via Image J. Transmission electron microscope imaging with an energy dispersive spectrometer (TEM/EDS) was performed with a JEM-2010HR with an accelerating voltage of 200 kV. X-ray photoelectron spectra (XPS) were obtained using an ESCA Lab250 device. UV spectra were obtained using a UV-3150 device. N_2 adsorption isotherms were obtained using an Autosorb-iQ2-MP device. X-ray diffraction (XRD) spectra were obtained using a D-MAX 2200 VPC. The Raman spectra were obtained using a Renishaw inVia laser micro-Raman spectrometer with 0.5% power of 17 mW, and a scanning time of 20 s × 2. The concentration of Ag in the dispersion was measured using inductively coupled plasma-optical emission spectrometry (SPECTRO CIROS VISION).

3 Results and discussion

3.1 Morphology of Ag nanocubes

An SEM image and a size-distribution plot of the silver nanocubes prepared via the two-step synthesis (the HNO_3 was injected when the UV absorption peak was placed at 409 nm, as shown in Fig. 5(e)) are shown in Figs. 1(a) and 1(b), respectively. It can be seen that the average side-edge length is approximately 66.7 nm, with a standard deviation of 6.6 nm. This result indicates successful control of the nanoparticle shape to a well-defined cubic morphology. Figures 1(c) and 1(d) show SEM images of the Ag nanoparticles during their shape evolution process, obtained for the sample collected when HNO_3 solution was just injected and 1 min after the selective etching process was initiated by the addition of NaCl, respectively. These results suggest that the shape of the nanoparticles, evolved from irregular (as shown in Fig. 1(c)) or quasi-cubic (as shown in Fig. 1(d)) morphologies, grow into well-defined cubic nanocrystals through this two-step synthesis process.

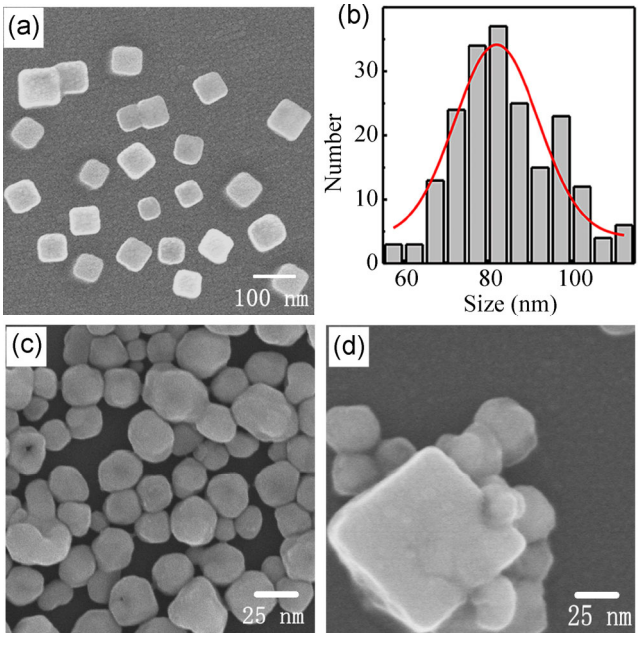

Figure 1 Representative SEM image (a) and size-distribution plot (b) of the Ag nanocubes synthesized via the two-step procedure; SEM images (c) and (d) of the Ag nanoparticles obtained after HNO_3 was just injected and 1 min after NaCl was injected, respectively.

3.2 Synthesis of Ag nanocubes via separated procedure

In order to study the mechanism of the shape evolution, we separated the two-step procedure into individual steps. The nanoparticles obtained from each step were centrifuged, washed, and collected before the pH value was tuned to ~1.5 using HNO_3. In this control experiment, there was no reductant (ethylal) present during the second step of Ag nanocube growth. Figure 2(a) shows a SEM image of the Ag INPs prepared through silver ammonia reduction and collected when the UV absorption peak was at 409 nm after reduction for 2 min. These particles have an average size of 32.1 nm with a standard deviation of 9.6 nm (Fig. 2(b)). The results reveal that the shapes of the nanoparticles are irregular, which is attributed to the fast and non-uniform silver ammonia reduction reaction [26, 37]. Figures 2(c) and 2(e) show representative SEM images of the Ag nanoparticles when the Ag INPs had reacted in the aqueous solution of PVP and HNO_3 collected 10 and 40 min after NaCl was injected, respectively. It is observed that the shape of the Ag nanoparticles had significantly evolved from

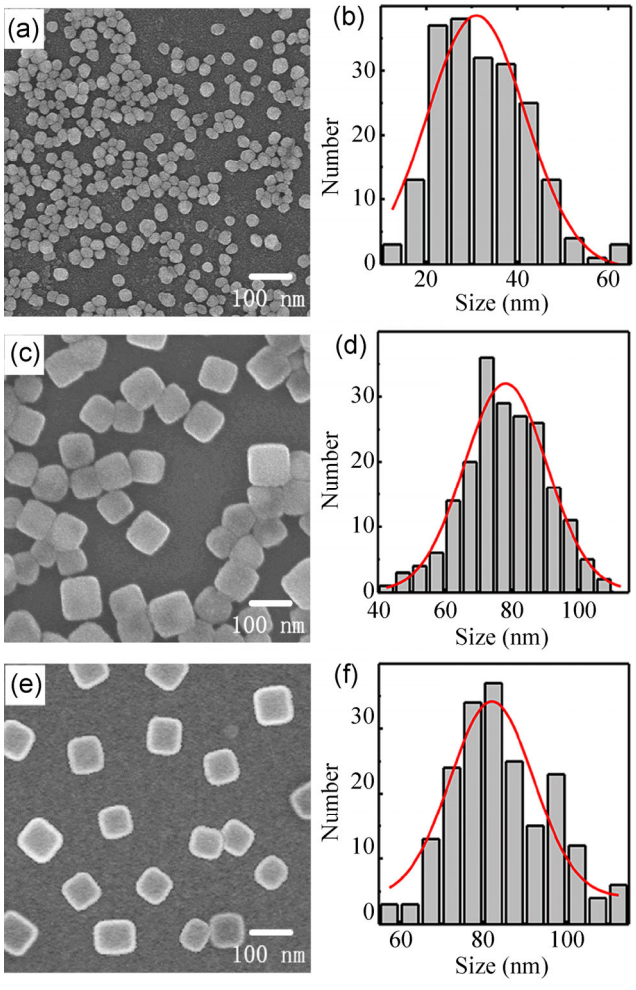

Figure 2 Representative SEM image (a) and size-distribution plot (b) of the Ag INPs. The inset shows the corresponding optical images of dispersion at the end time. Representative SEM images and size-distribution plots of the Ag nanoparticles after the INPs had been reacted in the aqueous solution of PVP and HNO_3 10 ((c) and (d)) and 40 min ((e) and (f)) after NaCl was injected, respectively.

irregular to cubic, and the average edge length of the Ag nanocubes is 84.5 nm, with a standard deviation of 11.9 nm (Fig. 2(f)). The size of the Ag nanocubes is much greater than that of the INPs, which indicates that the INPs had grown or agglomerated before they evolved to nanocubes. To slow this shape evolution, we conducted the reaction in an ice-water bath. Morphology changes were observed at various stages, with SEM images provided in Fig. S2 (in the Electronic Supplementary Material (ESM)). Considering that Ag^+ would not be reduced in the presence of sufficient HNO_3 and Cl^- as the oxidant etchants in the dispersion [38], the larger nanocubes are suggested to be a product

of the agglomeration of Ag INPs. The formation of the nanocube morphology would not simply be a product of Ag INP agglomeration; therefore, the Ag INP agglomerates underwent etching with HNO_3 to result in the final nanocube morphology. More importantly, taking the high shape monodispersity of the final products into consideration, the etching must be selective. Based on density functional theory (DFT), the Ag nanocubes enclosed by Ag {100} facets could selectively adsorb PVP molecules [39] that protect this surface facet during the etching process. Thus, the agglomerated Ag INPs were selectively etched to nanocubes with the protection of PVP. It is necessary to mention that if too much HNO_3 was injected (pH < 1), the nanoparticles would be over-etched, and the reaction solution would be become transparent after HNO_3 was injected for 1 h (Fig. S3(a) in the ESM). If the amount of HNO_3 was not sufficient (pH > 3.5), the etching reaction would not be initiated, and the INPs would not evolve to nanocubes (Fig. S3(b) in the ESM).

These results also suggest that the morphological evolution may be attributed to three processes: (i) formation of Ag INPs, (ii) agglomeration of INPs, and (iii) HNO_3 etching with PVP protection of the {100} facets. To investigate the effect of NaCl on the Ag nanocube preparation, we conducted a controlled experiment, in which the INPs were etched without the injection of NaCl. Figures 3(a) and 3(b) show the representative SEM image and size-distribution plot, respectively, of the Ag nanoparticles after the INPs had reacted in the aqueous solution of PVP and HNO_3 for 1 h without NaCl. It can be seen that the shape monodispersity was low and the average size of the nanoparticles was 39.7 nm (with a standard deviation of 14.4 nm), suggesting that only few INPs agglomerated and evolved to nanocubes. These results indicate that the major role of Cl^- was to promote the agglomeration of INPs in the shape-evolution process, as opposed to acting as a capping reagent. This is because the Ag nanoparticles should grow larger with a lesser amount of capping reagent. While no Cl^- exists, the INPs would adsorb Ag^+ owing to the common ion effect [40], thereby preventing their agglomeration due to the resultant electrostatic repulsion. On the other hand, with Cl^-, there are few Ag^+ on the surface of the

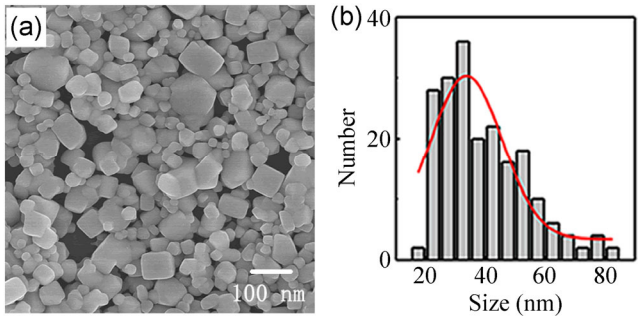

Figure 3 Representative SEM image (a) and size-distribution plot (b) of the Ag nanoparticles after INPs had reacted in the aqueous solution of PVP and HNO_3 for 1 h when Ag nanocubes could not be obtained without NaCl.

Ag INPs. Thus, the INPs could randomly agglomerate and avoid the influence of colloidal charges from Ag^+.

As the well-defined Ag nanocubes in this work were synthesized in the presence of Cl^-, we characterized the chlorine content in the final products using TEM/EDS and XPS measurements. Figure 4(a) shows the results of EDS, which was used as a semi-qualitative method to gauge atomic contents. The results suggest that Ag and Cl are the only species present in the nanocubes, with the other elemental signals arising from the support substrate (Cu, C, Si were from TEM grid, Cr was from device of the TEM, and the C chains in PVP are too stable to break and supply C to the Ag nanocubes). The qualitative results of elemental analysis via TEM/EDS were consistent with the results from the other 4 samples. The XPS results (Fig. 4(b)) indicate that the chlorine content was only 3.08 wt.% (the molar ratio was calculated using Eq. (S1) in the ESM) in the nanocubes and can be considered minimal. Moreover, the main Cl peaks were located below 199 eV, which implies that the Cl element should mainly be Cl^-. Taking into consideration the role of NaCl as the remover for the Ag^+ on the surface of the INPs, the Cl element in the Ag nanocubes could be attributed to the formation of AgCl on the surface of the nanoparticles. The XPS results are quantitative, and its unbroken spectrum is shown in Fig. S4 (in the ESM).

While NaCl is necessary to promote the agglomeration of Ag INPs, the Ag INPs could not directly evolve to nanocubes. Taking into consideration the importance of PVP protection for the morphological evolution, we supposed that PVP can only adsorb the Ag nanoparticles when their sizes were sufficiently

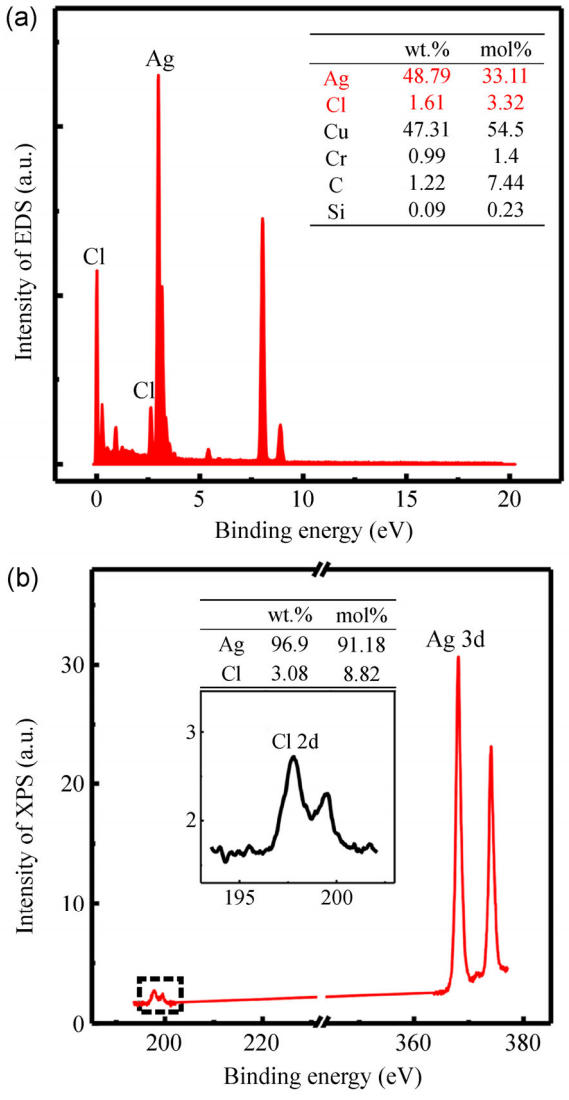

Figure 4 TEM/EDS (a) and XPS (b) spectra of the Ag nanocubes synthesized in the presence of NaCl.

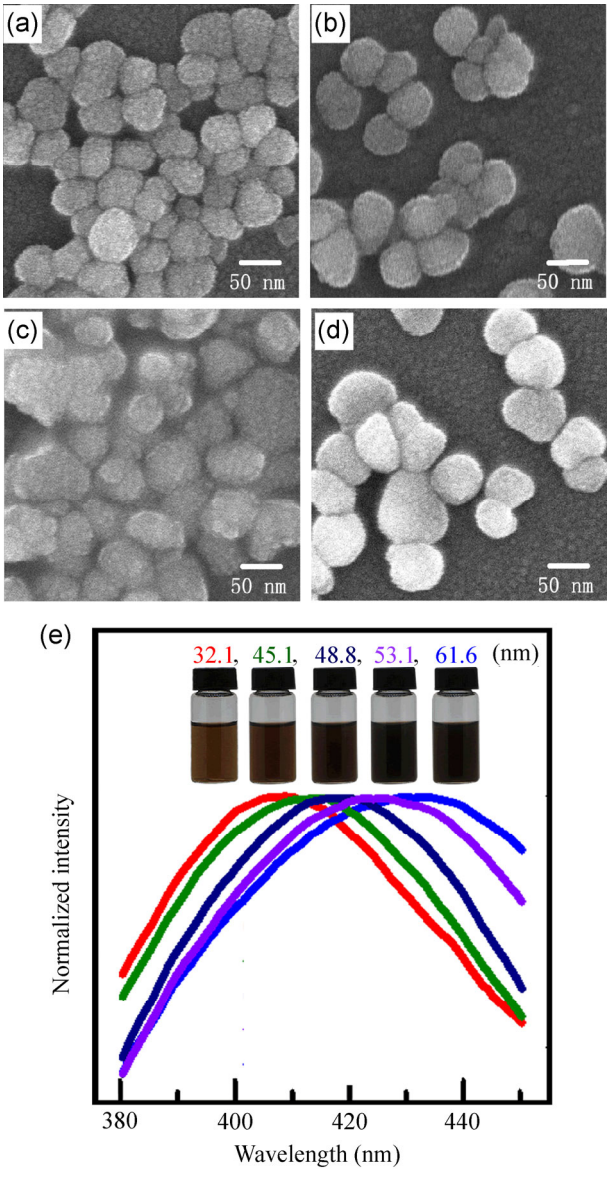

Figure 5 SEM images of INPs with average sizes of 45.1 (a), 48.8 (b), 53.1 (c), and 61.6 nm (d) obtained by controlling the reaction times after the injection of ammonia solution and before the injection of HNO_3. The UV spectra of the reaction dispersions (e), from which INPs shown in (a)–(d) and Fig. 2(a) were obtained. The insets of (e) show the colors of the reaction dispersions before HNO_3 was injected.

large. In order to characterize the protective ability of PVP quantitatively, we measured the zeta potentials of INPs in the aqueous solution of 1.2×10^{-2} mol·L^{-1} $AgNO_3$ with the pH value tuned to ~1.5 with HNO_3 before and after the injection of 150 mmol·L^{-1} PVP. The average size of the INPs was tuned from 32.1 (Fig. 2(a)) to 45.1 (Fig. 5(a)), 48.8 (Fig. 5(b)), 53.1 (Fig. 5(c)), and 61.6 nm (Fig. 5(d)) by injecting HNO_3 when the UV absorption peak appears at 409, 414, 416, 425, and 429 nm, respectively. Figures S5(a)–S5(d) in the ESM show the size-distribution plots of the nanoparticles shown in Figs. 5(a)–5(d), respectively. Figure 5(e) shows UV spectra of the reaction dispersions, from which the INPs shown in Figs. 2(a) and 5(a)–5(d) were obtained. The insets of Fig. 5(e) show the colors of the reaction dispersions before HNO_3 was injected. The results of Fig. 6 suggest that the zeta potential decreases with an increase in the average size of INPs before the injection of PVP. However, the absolute value of the change of zeta potential rapidly increases as the average size of INPs exceeds ~50 nm after the injection of PVP. These results indicate that the adsorption and

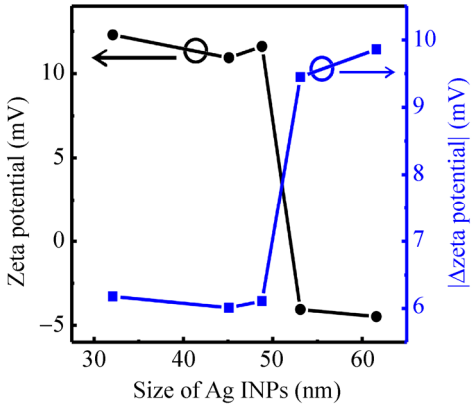

Figure 6 Relationship between the zeta potentials of the INPs in the aqueous solution of 1.2 mol·L^{-1} $AgNO_3$ with pH value tuned to 1.5 using HNO_3 and the average size of INPs (black); relationship between the absolute value of the change of zeta potentials after the injection of 150 mol·L^{-1} PVP (blue) and the average size of INPs.

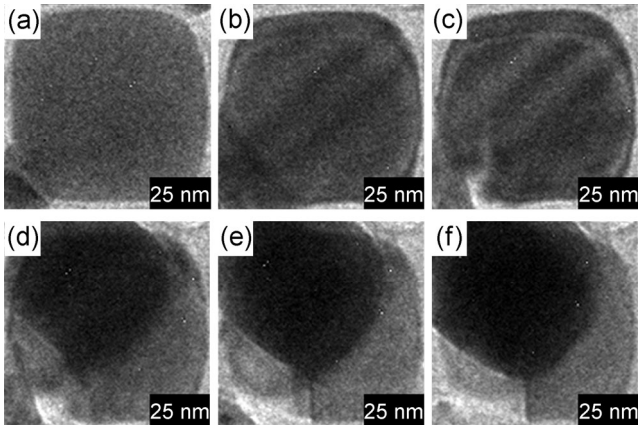

Figure 7 (a)–(f) The TEM images of a nanocube irradiated with a 200-kV electron beam for 2, 4, 6, 10, 12, and 14 s.

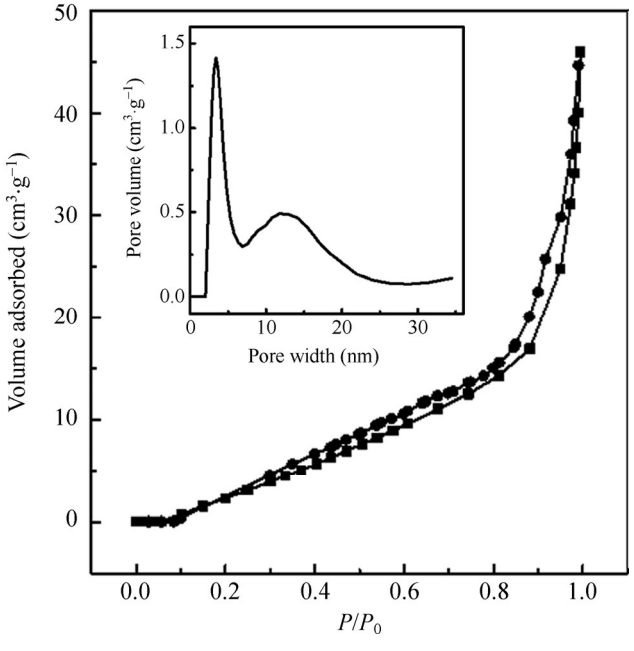

Figure 8 N_2 adsorption isotherm for Ag nanocubes and the corresponding pore-size distribution (inset).

protective abilities of PVP become dominant when the size of INPs reaches ~50 nm, which is in agreement with the fact that there were few nanocubes with sizes <50 nm.

It is worth noting that we could not obtain TEM or high-resolution TEM (HRTEM) images of the nanocubes, because they could not keep their shape stable under the 200-kV electron beam. Figures 7(a)–7(f) show the TEM images of a nanocube irradiated using a 200-kV electron beam for 2, 4, 6, 10, 12, and 14 s, respectively. This phenomenon is characteristic of some hollow structure [41]. Thus, we supposed that the nanocubes contained many defects or even pores caused by the imperfect packing during the agglomeration of Ag INPs. The pores were characterized using the N_2 adsorption test (Fig. 8). According to the International Union of Pure and Applied Chemistry (IUPAC) [42] nomenclature, the resulting isotherm can be classified as a type-V isotherm, and the hysteresis loop can be classified as a type of slit mesopore. The corresponding size distribution data calculated from the nitrogen adsorption isotherm using the Barrett–Joyner–Halenda (BJH) method reveals that the pores inside the Ag nanocubes were mainly slit mesopores with a pore-size distribution centered at 8.5 and 29.4 nm (Fig. 8 inset). The BET specific surface area of the Ag nanocubes was found to be 13.463 m^2·g^{-1}.

Figure 9 shows the XRD pattern of Ag nanocubes. Apart from the dominant Ag(111) peak, Ag(220), Ag(311), and Ag(222) peaks were found at 2θ values of 38.1, 64.4, 77.5, and 81.5, respectively. This result is in good agreement with the assumption for pores inside the Ag nanocubes, which indicates that during the agglomeration of the Ag INP, unavoidable imperfect packing would result in the formation of slit pores between their surfaces. The XRD patterns, SEM image, and size-distribution plot of Ag nanocubes synthesized via conventional high-temperature/glycol method [38] are shown in Figs. S6(a)–S6(c) (in the ESM), respectively.

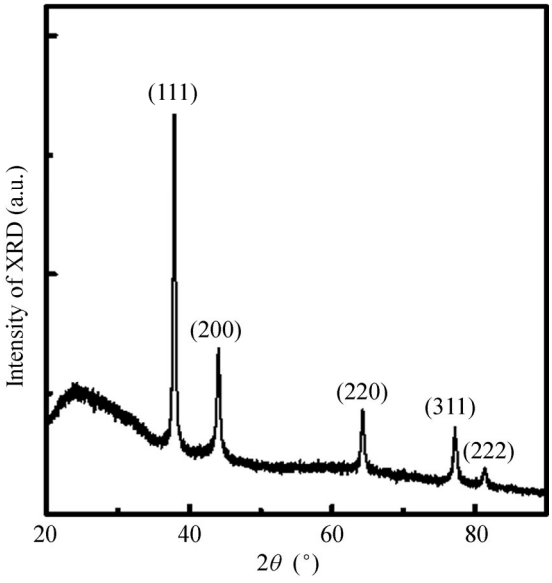

Figure 9 XRD patterns of the Ag nanocubes.

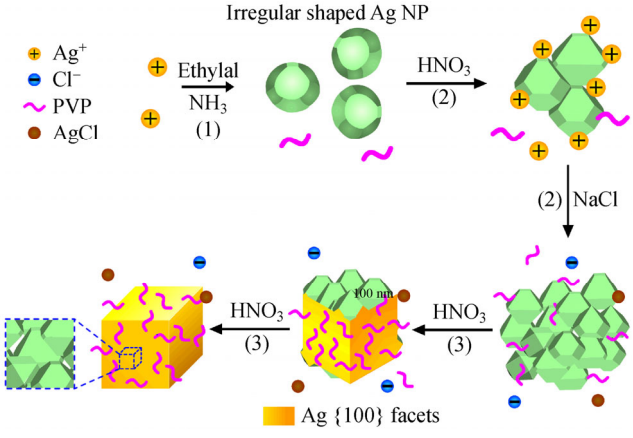

Figure 10 Schematic illustration summarizing the evolution of Ag nanocubes from Ag INPs via HNO_3 etching. The major steps include: (1) the formation of Ag INPs; (2) the agglomeration of Ag INPs; and (3) selective etching. The agglomeration process was confirmed through SEM measurement.

3.3 Formation mechanism of Ag nanocubes

Figure 10 schematically illustrates how Ag nanoparticles evolved from INPs to nanocubes. This process comprises three distinct steps: (1) the formation of Ag INPs, whereby $AgNO_3$ was reduced to Ag INPs by ethylal in the alkaline media; (2) the agglomeration of Ag INPs in the acid system, with INPs etched by HNO_3. Once similar lattice planes were etched out on the surfaces of two or more INPs with little surface charge, they would agglomerate because of the high specific surface energy of the small nanoparticles. It should be noted that Ag^+ was continually produced by etching. When the INPs adsorbed too much Ag^+ through the common ion effect [40], they would not agglomerate because of the electrostatic repulsive force, even if they have similar surface lattice planes. Then, the Cl^- (if injected) would react with Ag^+. Consequently, the surface charges of the INPs decrease, causing all of the INPs to agglomerate randomly and the size of the nanocubes obtained in the end to be normally distributed. (3) Selective etching, whereby the PVP protection of the nanoparticles became stronger during the growth of nanoparticles by agglomeration. Specifically, when the sizes of the nanoparticles were sufficiently large, PVP would be adsorbed strongly on the facets [39] to decrease the etching rate on the facets. Consequently, the non-{100} facets were etched, and the nanoparticles were inevitably enclosed by Ag {100} facets after the reaction.

3.4 Tuning the size of Ag nanocubes

The average size of the Ag nanocubes synthesized via the two-step procedure was less than those of the Ag nanocubes synthesized via the separated procedure. This is likely because the separated procedure results in a loss of some extremely small residual nanoparticles that could not be obtained through centrifugation. Taking this loss into account, it is very likely that the size of the Ag nanocubes can be controlled by fine tuning the initial size of the INPs. Thus, we etched the Ag INPs with different sizes. Consequently, Ag nanocubes with varying sizes were obtained. Specifically, Ag nanocubes with average edge lengths of 66.7 (Fig. 11 inset (a)), 74.5 (Fig. 11 inset (b)), 92.0 (Fig. 11 inset (c)), 102.4 (Fig. 11 inset (d)), and 130.7 nm (Fig. 11 inset (e)) were obtained by etching INPs with average sizes of 32.1 (Fig. 2(a)), 45.1 (Fig. 5(a)), 48.8 (Fig. 5(b)), 53.1 (Fig. 5(c)), and 61.6 nm (Fig. 5(d)), respectively. It is revealed that the average edge length of nanocubes increases with increase in the average size of the primary INPs. The size-distribution plots of the nanoparticles shown in Fig. 11 inset are shown in Fig. S5 in the ESM.

3.5 SERS application

Finally, we applied the Ag nanocubes in the SERS field. The SERS substrates were fabricated by dropping an aqueous dispersion of Ag nanocubes (with an average

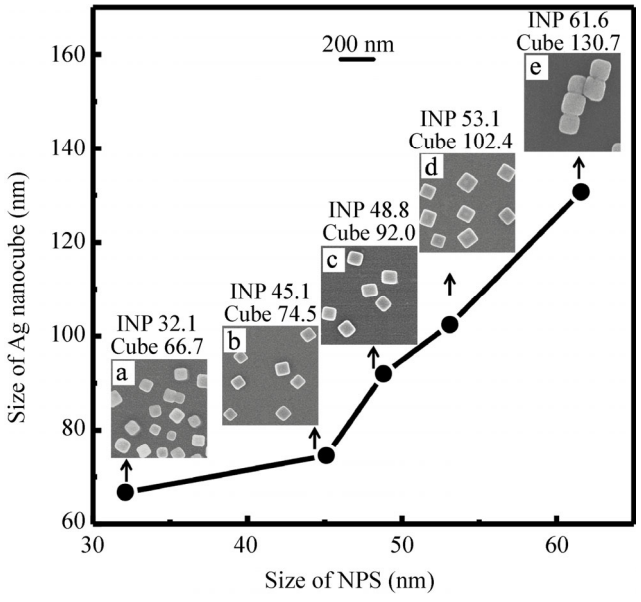

Figure 11 Relationship between the average edge length of nanocubes and the average size of INPs; the insets (a)–(e) are SEM images of Ag nanocubes obtained by etching the INPs with sizes of 32.1 (a), 45.1 (b), 48.8 (c), 53.1 (d) and 61.6 nm (e), respectively.

size of 130.7 nm and concentration of 5.11×10^{-4} mg·L^{-1}) followed by coating and drying in vacuum. Then, 3 μL aqueous solution of R6G was coated on the substrates. Figure 12 shows the Raman spectrum of 10^{-3} mol·L^{-1} R6G without an Ag substrate, and the inset shows the characteristic peaks of R6G at 1,363 and 1,511 cm^{-1}. Figure 13(a) shows the Raman spectra of R6G of different concentrations (10^{-6}, 10^{-14}, and 10^{-16} mol·L^{-1}) with Ag substrates. We found that the detection limit could be as low as 10^{-16} mol·L^{-1} on using the newly developed mesoporous Ag nanocubes. This is determined by comparing the peak area of the spectra for 10^{-16} mol·L^{-1} and that without the Ag substrate at 1,363 and 1,511 cm^{-1}, respectively. Then, by using equation (1), the SERS enhancement factor was calculated [43] as 10^{13}. In addition, we measured the Raman spectra of R6G of different concentrations (10^{-10}, 10^{-12}, and 10^{-13} mol·L^{-1}) with substrates of Ag nanocubes with an average size of 123.9 nm (Fig. S1(c) in the ESM) and concentration of 4.19×10^{-4} mg·L^{-1}) synthesized via the conventional high-temperature/glycol method [38], as shown in Fig. 13(b). It was found that when the concentration of R6G was as low as 10^{-13} mol·L^{-1}, the detection limit of R6G with conventional Ag-nanocube substrates could only be 10^{-12} mol·L^{-1}, which was

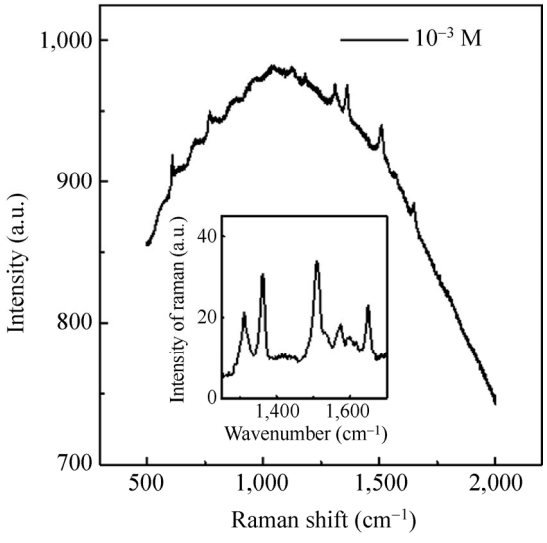

Figure 12 Raman spectrum of R6G without Ag substrates.

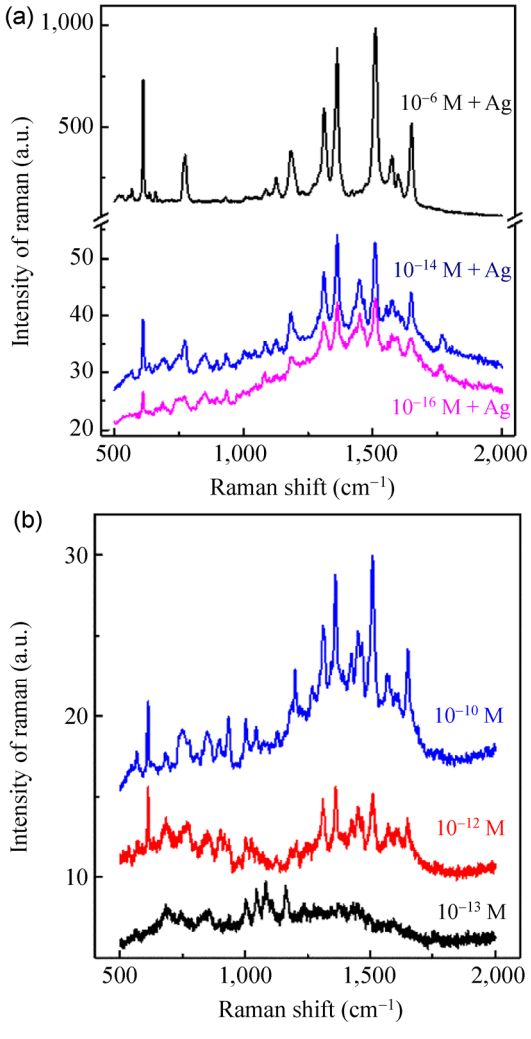

Figure 13 (a) Raman spectrum of R6G with our Ag-nanocube substrates and (b) Raman spectrum of R6G with conventional Ag-nanocube substrates.

consistent with the results of a previous study [44]. It is necessary to mention that gap structures had been reported to be able to enhance the local electromagnetic field [45–47] and increase the SERS enhancement factor, and the slit pores in our Ag nanocubes were similar to gap structures. Thus, we attributed the significant decrease in the detection limit of R6G with our Ag-nanocube substrates compared to the detection limit with conventional Ag nanocubes to the slit pores in our nanocubes.

$$EF = (I_{sers} \times N_{normal})/(I_{normal} \times N_{sers}) \quad (1)$$

4 Conclusions

In this work, we developed a facile synthetic approach to prepare Ag nanocubes at room temperature in a water phase through selective oxidative etching of Ag INPs. During the etching process, PVP is strongly adsorbed on the {100} facets of Ag, providing protection for etching with HNO_3 and Cl^- species. Consequently, Ag nanocubes with well-defined morphologies enclosed by the {100} facets were obtained. Meanwhile, the Ag nanoparticles would inevitably agglomerate, leading to an increase in the size of Ag nanoparticles. However, when the Ag nanoparticles adsorbed relatively high amounts of Ag^+ owing to the common ion effect, their tendency to agglomerate dramatically decreases because of the electrostatic repulsive force, and the agglomeration, if at all, would be irregular. Thus, in order to deplete the Ag^+ in the solution, Cl^- was injected during the etching process. Consequently, both the size and shape monodispersity were enhanced. Moreover, the agglomeration was necessary to some extent for the selective oxidation of Ag nanoparticles because PVP could not effectively protect the Ag nanoparticles from the oxidative etching when their sizes were below approximately 50 nm. Additionally, because of the unavoidable imperfect packing of Ag INPs during agglomeration, mesopores were formed inside the Ag nanocubes, which were confirmed by N_2 adsorption/desorption measurement. Finally, the Ag nanocubes were used to enhance the Raman signal of R6G and lower the detection limit of R6G to 10^{-16} mol·L^{-1}, which is much lower than the detection limit with conventional Ag-nanocube (synthesized via the high temperature/glycol method) substrates (10^{-12} mol·L^{-1}). The significant enhancement is likely due to the slit pores similar to gap structures between metallic nanoparticles.

Acknowledgements

X. D. C is grateful to the National Natural Science Foundation of China (No. 51233008). G. F. C. gratefully acknowledges the financial support by the National Natural Science Foundation of China (Nos. 51271205 and 50801070), Guangzhou Pearl Technology the Nova Special Project (No. 2012J2200058), Excellent Young College Teachers Development Program in Guangdong Province (No. Yq2013006), Research and Application of Key Technologies Oriented the Industrial Development (Nos. 90035-3283309 and 90035-3283321), Science and Technology Plan Projects of Guangzhou city (No. 2013Y2-00102), Huizhou city (No. 2012B050013012) and DaYa Gulf district of Huizhou city (No. 20110108 and 20120212). G. W. acknowledges the financial support from the start-up funding of University at Buffalo, SUNY.

Electronic Supplementary Material: Supplementary material (high-resolution SEM image of the silver nanocubes; the SEM images of the nanoparticles 0.5, 1, and 1.5 h after HNO_3 was injected when the reaction solution was bathed in ice water; photo/SEM image of nanoparticles synthesized when the pH was tuned to 1/3.5; unbroken XPS spectrum of the Ag nanocubes; size-distribution plots of the nanoparticles shown in Figs. 5(a)–5(d), 11 inset (b), 11 inset (c), 11 inset (d), and 11 inset (e); XRD patterns, SEM image, and size-distribution plot of the Ag nanocubes synthesized via conventional high-temperature/glycol method) is available in the online version of this article at http://dx.doi.org/10.1007/s12274-015-0745-7.

References

[1] Lee, S. Y.; Hung, L.; Lang, G. S.; Cornett, J. E.; Mayergoyz, I. D.; Rabin, O. Dispersion in the SERS enhancement with silver nanocube dimers. *ACS Nano* **2010**, *4*, 5763–5772.

[2] Park, H. G.; Joo, J. H.; Kim, H. G.; Lee, J. S. Shape-dependent reversible assembly properties of polyvalent DNA-silver nanocube conjugates. *J. Phys. Chem. C* **2012**, *116*, 2278–2284.

[3] Mahmoud, M. A.; Chamanzar, M.; Adibi, A.; El-Sayed, M. A. Effect of the dielectric constant of the surrounding medium and the substrate on the surface plasmon resonances and sensitivity factors of highly symmetric systems: Silver nanocubes. *J. Am. Chem. Soc.* **2012**, *134*, 6434–6342.

[4] Ahamad, N.; Bottomley, A.; Ianoul, A. Optimizing refractive index sensitivity of supported silver nanocube monolayers. *J. Phys. Chem. C* **2012**, *116*, 185–192.

[5] Haes, A. J.; Zou, S.; Schatz, G. C.; Van Duyne, R. P. A nanocscale optical biosensor: The long range distance dependence of the localized surface plasmon resonance of noble metal nanoparticles. *J. Phys. Chem. B* **2004**, *108*, 109–116.

[6] Whitney, A. V.; Elam, J. W.; Zou, S.; Zinovev, A. V.; Stair, P. C.; Schatz, G. C.; Van Duyne, R. P. Localized surface plasmon resonance nanosensor: A high-resolution distance-dependence study using atomic layer deposition. *J. Phys. Chem. B* **2005**, *109*, 20522–20528.

[7] Jain, P. K.; Huang, W.; El-Sayed, M. A. On the universal scaling behavior of the distance decay of plasmon coupling in metal nanoparticle pairs: A plasmon ruler equation. *Nano Lett.* **2007**, *7*, 2080–2088.

[8] Sun, Y. G.; Xia, Y. N. Shape-controlled of gold and silver nanoparticles. *Science* **2002**, *298*, 2176–2179.

[9] Tao, A.; Sinsermsuksakul, P.; Yang, P. D. Tunable plasmonic lattices of silver nanocrystals. *Nat. Nanotechnol.* **2007**, *2*, 435–440.

[10] Mahmoud, M. A.; Tabor, C. E.; El-Sayed, M. A. Surface-enhanced Raman scattering enhancement by aggregated silver nanocube monolayers assembled by the Langmuir-Blodgett technique at different surface pressures. *J. Phys. Chem. C* **2009**, *113*, 5493–5501.

[11] Ling, X. Y.; Yan, R.; Lo, S.; Hoang, D. T.; Liu, C.; Fardy, M. A.; Khan, S. B.; Asiri, A. M.; Bawaked, S. M.; Yang, P. Alumina-coated Ag nanocrystal monolayers as surface enhanced Raman spectroscopy platforms for the direct spectroscopic detection of water splitting reaction intermediates. *Nano Res.* **2014**, *7*, 132–143.

[12] Wang, Y.; Lu, N.; Wang, W.; Liu, L.; Feng, L.; Zeng, Z.; Li, H.; Xu, W.; Wu, Z.; Hu, W.; Lu, Y.; Chi, L. Highly effective and reproducible surface-enhanced Raman scattering substrates based on Ag pyramidal arrays. *Nano Res.* **2013**, *6*, 159–166.

[13] Mahmoud, M. A.; El-Sayed, M. A. Comparative study of the assemblies and the resulting plasmon fields of Langmuir-Blodgett assembled monolayers of silver nanocubes and gold nanocages. *J. Phys. Chem. C* **2008**, *112*, 14618–14625.

[14] Wen, X. L.; Yi, M. F.; Zhang, D. G.; Wang, P.; Lu, Y. H.; Ming, H. Tunable plasmonic coupling between silver nano-cubes and silver nano-hole arrays. *Nanotechnology* **2011**, *22*, 085203–085209.

[15] Galush, W. J.; Shelby, S. A.; Mulvihill, M. J.; Tao, A.; Yang, P. D.; Groves, J. T. A nanocube plasmonic sensor for molecular binding on membrane surfaces. *Nano Lett.* **2009**, *9*, 2077–2082.

[16] Wu, H. J.; Henzie, J.; Lin, W. C.; Rhodes, C.; Li, Z.; Sartorel, E.; Thorner, J.; Yang, P. D.; Groves, J. T. Membrane-protein binding measured with solution-phase plasmonic nanocube sensors. *Nat. Methods* **2012**, *9*, 1189–1191.

[17] Mahmoud, M. A.; Poncheri, A. J.; Phillips, R. L.; El-Sayed, M. A. Plasmonic field enhancement of the exciton-exciton annihilation process in a poly(p-phenyleneethylene) fluorescent polymer by Ag nanocubes. *J. Am. Chem. Soc.* **2010**, *132*, 2633–2641.

[18] Yi, M. F.; Zhang, D. G.; Wen, X. L.; Fu, Q.; Wang, P.; Lu, Y. H.; Ming, H. Fluorescence enhancement caused by plasmonics coupling between silver nano-cubes and silver film. *Plasmonics* **2011**, *6*, 213–217.

[19] Han, S. B.; Song, Y. J.; Lee, J. M.; Kim, J. Y.; Park, K. W. Platinum nanotube catalysts for methanol and ethanol electrooxidation. *Electrochem. Commun.* **2008**, *10*, 1044–1047.

[20] Wang, C.; Daimon, H.; Lee, Y.; Kim, J.; Sun, S. H. Synthesis of monodisperse Pt nanocubes and their enhanced catalysis for oxygen reduction. *J. Am. Chem. Soc.* **2007**, *129*, 6974–6975.

[21] Lee, C. L.; Tsai, Y. L.; Chen, C. W. Specific and mass activity of silver nanocube and nanoparticle-based catalysts for electroless copper deposition. *Electrochim. Acta* **2013**, *104*, 185–190.

[22] Xu, R.; Wang, D. S.; Zhang, J. T.; Li, Y. D. Shape-dependent catalytic activity of silver nanoparticles for the oxidation of styrene. *Chem. Asian J.* **2006**, *1*, 888–893.

[23] Skrabalak, S. E.; Au, L.; Li, X. D.; Xia, Y. N. Facile synthesis of Ag nanocubes and Au nanocages. *Nat. Protoc.* **2007**, *2*, 2182–2190.

[24] Lu, X. M.; Au, L.; McLellan, J.; Li, Z. Y.; Marquez, M.; Xia, Y. N. Fabrication of cubic nanocages and nanoframes by dealloying Au/Ag alloy nanoboxes with aqueous etchant based on $Fe(NO_3)_3$ or NH_4OH. *Nano Lett.* **2007**, *7*, 1764–1769.

[25] Ping, H. M.; Chen, Y. Z.; Guo, H. Z.; Wang, Z. W.; Zeng, D. Q.; Wang, L. S.; Peng, D. L. A facile solution approach for the preparation of Ag@Ni core-shell nanocubes. *Mater. Lett.* **2014**, *116*, 239–242.

[26] Xia, Y. N.; Xia, X. H.; Wang, Y.; Xie, S. F. Shape-controlled synthesis of metal nanocrystals. *MRS Bull.* **2013**, *38*, 335–344.

[27] Zhang, Q.; Li, W. Y.; Moran, C.; Zeng, J.; Chen, J. Y.; Wen, L. P.; Xia, Y. N. Seed-mediated synthesis of Ag nanocubes with controllable edge lengths in the range of 30-200 nm and comparison of their optical properties. *J. Am. Chem. Soc.* **2010**, *132*, 11372–11378.

[28] Galush, W. J.; Shelby, S. A.; Mulvihill, M. J.; Tao, A.; Yang, P.; Groves, J. T. Polyol synthesis of silver nanoparticles: Use of chloride and oxygen to promote the formation of single-crystal, truncated cubes and tetrahedrons. *Nano Lett.* **2009**, *9*, 2077–2082.

[29] Zhang, Q.; Cobley, C.; Au, L.; McKiernan, M.; Schwartz, A.; Wen, L. P.; Chen, J. Y.; Xia, Y. N. Production of Ag nanocubes on a scale of 0.1 g per batch by protecting the NaHS-mediated polyol synthesis with argon. *ACS Appl. Mater. Inter.* **2009**, *1*, 2044–2048.

[30] Rycenga, M.; McLellan, J. M.; Xia, Y. N. Controlling the assembly of silver nanocubes through selective functionalization of their faces. *Adv. Mater.* **2008**, 20, 2416–2420.

[31] Yu, D. B.; Yam, V. W. Controlled synthesis of monodisperse silver nanocubes in water. *J. Am. Chem. Soc.* **2004**, *126*, 13200–13201.

[32] Chang, Y. M.; Lu, I. T.; Chen, C. Y.; Hsieh, Y. C.; Wu, P. W. High-yield water-based synthesis of truncated silver nanocubes. *J. Alloy. Compd.* **2014**, *586*, 507–511.

[33] Leopold, N.; Lendl, B. A new method for fast preparation of highly surface-enhanced Raman scattering (SERS) active silver colloids at room temperature by reduction of silver nitrate with hydroxylamine hydrochloride. *J. Phys. Chem. B* **2003**, *107*, 5723–5727.

[34] Mahapatra, S. K.; Bogle, K. A.; Dhole, S. D.; Bhoraskar, V. N. Synthesis of gold and silver nanoparticles by electron irradiation at 5–15 keV energy. *Nanotechnology* **2007**, *18*, 135602.

[35] Maity, D.; Kanti, B. M.; Bhowmick, B.; Sarkar, J.; Saha, S.; Acharya, K.; Chakraborty, M.; Chattopadhyay, D. *In situ* synthesis, characterization, and antimicrobial activity of silver nanoparticles using water soluble polymer. *J. Appl. Polym. Sci.* **2011**, *122*, 2189–2196.

[36] Zhang, F.; Wu, X.; Chen, Y.; Lin, H. Synthesis and characterization of stable aqueous dispersions of silver nanoparticles through the Tollens process. *Fiber. Polym.* **2009**, *10*, 496–501.

[37] Yin, Y. D.; Li, Z. Y.; Zhong, Z. Y.; Gates, B.; Xia, Y. N.; Venkateswaran, S. Large-scale synthesis of silver nanocubes: The role of HCl in promoting cube perfection and monodispersity. *J. Mater. Chem.* **2002**, *12*, 522–527.

[38] Im, S. H.; Lee, Y. T.; Wiley, B.; Xia, Y. Large-scale synthesis of silver nanocubes: The role of HCl in promoting cube perfection and monodispersity**.** *Angew. Chem. Int. Ed.* **2005**, *44*, 2154–2157.

[39] Xia, X. H.; Zeng, J.; Zhang, Q.; Moran, C. H.; Xia, Y. N. Recent developments in shapes-controlled synthesis of silver nanocrystals. *J. Phys. Chem. C* **2012**, *116*, 21647–21656.

[40] Chen, A. H.; Xie, H. X.; Wang, H. Q.; Li, H. Y.; Li, X. Y. Fabrication of Ag/polypyrrole coaxial nanocables through common ions adsorption effect. *Synthetic Met.* **2006**, *156*, 346–350.

[41] Ai, L. H.; Zhang, C. H.; Jiang, J. Hierarchical porous AgCl@Ag hollow architectures: Self-templating synthesis and highly enhanced visible light photocatalytic activity. *Appl. Catal. B-Environ.* **2013**, *142,* 744–751.

[42] Sing, K. S. W. D.; Everett, H.; Haul, R. A. W.; Moscou, L.; Pierotti, R. A.; Rouquerol, J.; Siemieniew, T. Reporting physisorption data for gas/solid systems with special reference to the determination of surface area and porosity. *Pure Appl. Chem.* **1985**, *57*, 603–619.

[43] Orendorff, C. J.; Gole, A.; Sau, T. K.; Murphy, C. J. Surface-enhanced Raman spectroscopy of self-assembled monolayers: Sandwich architecture and nanoparticles shape dependence. *Anal. Chem.* **2005**, *77*, 3261–3266.

[44] Huang, Z. L.; Meng, G. W.; Huang, Q.; Chen, B.; Zhou, F.; Hu, X. Y.; Qian, Y. W.; Tang, H. B.; Han, F. M.; Chu, Z. Q. Highly effective and reproducible surface-enhanced Raman scattering substrates based on Ag pyramidal arrays. *Nano Res.* **2014**, *7*, 1177–1187.

[45] Qin, L. D.; Zou, S. L.; Xue, C.; Atkinson, A.; Schatz, G. C.; Mirkin, C. A. Designing, fabrication, and imaging Raman hot spots. *Proc. Natl. Acad. Sci. USA* **2006**, *103*, 13300–13303.

[46] Pedano, M. L.; Li, S. Z.; Schatz, G. C.; Minkin, C. A. Periodic electric field enhancement along gold rods with nanogaps. *Angew. Chem. Int. Ed.* **2010**, *49*, 78–82.

[47] Li, S. Z.; Pedano, M. L.; Chang, S. H.; Minkin, C. A.; Schatz, G. C. Gap structure effects on surface-enhanced Raman scattering intensities for gold gapped rods. *Nano Lett.* **2010**, *10*, 1722–1727.